Regional Climate Studies

Series Editors: H.-J. Bolle, M. Menenti, I. Rasool

Hans-Jürgen Bolle, Matthias Eckardt,
Dirk Koslowsky, Fabio Maselli, Joaquín Meliá
Miralles, Massimo Menenti, Folke-Sören Olesen,
Ljiljana Petkov, Ichtiaque Rasool,
Adriaan Van de Griend (Eds.)

Mediterranean Land-surface Processes Assessed From Space

With 442 Figures, 320 in colour

Springer

Editors

Hans-Jürgen Bolle, Dr., Prof. a. D.
Stücklenstrasse 18 c
81247 München, Germany

Matthias Eckardt, Dipl. Met.
Freie Universität Berlin, Institut für Meteorologie
Carl-Heinrich-Becker-Weg 6-10
12165 Berlin, Germany

Dirk Koslowsky, Dr.
Freie Universität Berlin, Institut für Meteorologie
Carl-Heinrich-Becker-Weg 6-10
12165 Berlin, Germany

Fabio Maselli, Dr.
CNR - Istituto di Biometeorologia (IBIMET)
Piazzale delle Cascine 18
50144 Firenze, Italy

Joaquín Meliá Miralles, Dr., Prof.
Universitat de Valencia, Facultat de Física
Dpt. de Termodinàmica, Remote Sensing Unit
Calle Dr. Moliner, 50, Burjassot
46100 Valencia, Spain

Massimo Menenti, Dr., Prof.
CNR - Istituto Per I Sistemi Agricoli E Forestali
Del Mediterraneo - ISAFoM,
P.O. Box 101
80040 S. Sebastiano al Vesuvio (NA), Italy

Folke-Sören Olesen, Dipl. Met.
Forschungszentrum Karlsruhe
Institut für Meteorologie und Klimaforschung
Postfach 3640
76133 Karlsruhe, Germany

Ljiljana Petkov, Dr.
Adriaan van Ostadelaan, 5
2343 EL Oegstgeest, The Netherlands

Ichtiaque Rasool, Dr.
60 Quai Louis Blèriot
75016 Paris, France

Adriaan A. Van de Griend, Dr., Prof. Em.
Guido Gezellelaan 38
3705 AT Zeist, The Netherlands

ISBN 10 3-540-40151-2 Springer Berlin Heidelberg New York
ISBN 13 978-3-540-40151-3 Springer Berlin Heidelberg New York

Library of Congress Control Number: 2006927434

Springer is part of Springer Science+Business Media
springeronline.com

Cover design: E. Kirchner, Heidelberg
Production: A. Oelschläger
Typesetting: Camera-ready by the Editors

Printed on acid-free paper 30/2132/AO 54321

Contributing Authors

Heiner Billing

Freie Universität Berlin, Institut für Meteorologie
Carl-Heinrich-Becker-Weg 6-8
12165 Berlin, Germany

Anatoly Gitelson

Ben-Gurion University of the Negev
Remote Sensing Laboratory
Sede-Boker Campus, 84990 Israel

Frank Göttsche

Hermann-von-Helmholtz-Platz 1
76344 Eggenstein-Leopoldshafen, Germany

Anne Jochum-Osann
Alphaclim
Zapateros, 15-7
02005 Albacete, Spain

Ernesto López-Baeza

Remote Sensing Unit, Dptm. de Termodinàmica
Facultat de Física, Universitat de Valencia
Calle Dr. Moliner, 50, Burjassot
46100 Valencia, Spain

Francesco Meneguzzo

CNR - Istituto di Biometeorologia (IBIMET)
via Giovanni Caproni 8, 50145 Firenze, Italy

Jose Moreno

Department of Thermodynamics, Faculty of Physics
University of Valencia
46100 Burjassot, Valencia, Spain

Françoise Nerry

Laboratoire des Sciences de l´Image
et de la Télédétection, ENSPS/LSIIT
University L. Pasteur, Strasbourg 1
Boulevard Sebastien Brandt
67400 Illkirch, France

Paolo Rossini

Studio PAN Ricerche
Viale Regina Margherita 270
00198 Roma, Italia

Frank Veroustraete

Flemish Institute for Technological Research - VITO
Centre for Remote Sensing and Atmospheric Processes TAP
Boeretang 200, 2400 Mol, Belgium

Roland Vogt

University of Basel, Department of Geography
Institut für Meteorologie, Klimatologie.
und Fernerkundung., MCR Lab
Spalenring 145
4055 Basel, Schweiz

Peter J. Van Oevelen

European Space Agency
European Space Research & Technology Centre
ESA - ESTEC, Mission Experts Division
Land Surfaces Unit (EOP - SML)
P.O. Box 299, 2200 AG Noordwijk zh
The Netherlands

Preface

Observations from space have been an important component in a number of research projects of the European Commission aiming, in the context of “Global Change”, at the assessment of land-surface processes and their changes in the Mediterranean area. With the new generation of satellites, carrying improved instrumentation, these observations will gain in importance in the future. Changes in the Mediterranean environment are linked to the global climate system which is characterized by a strong inherent interannual variability but may, in addition, undergo trends that develop slowly in time. To assess, to which degree Mediterranean land-surface processes such as aridification, desertification, soil quality and changes of water resources are affected by the development of the global climate system, it is necessary to extend such studies over long time periods which would allow to average over the “noise” in the signals caused by its natural variability. Presently time series of thirty years are found adequate to distinguish shorter term fluctuations from long term trends and to draw reliable conclusions from those data.

For two reasons it seems now timely to summarize recent experience in dealing with satellite data when studying changes at the land surfaces. Firstly, to document the results obtained so far and secondly to pave the ground for a smooth transition from old sensor systems to the advanced ones which are already available or will soon become operational. From the new sensor systems, reliable long time series will become available only thirty years from now. In combination with existing data sets this goal can be accomplished in fifteen years from now. To create a coherent data set of the required length it is mandatory to fit the new measurements with their different instrumental parameters to the present data series.

The information content of measurements made from space can only fully be understood and applied if the physical and - in the case of vegetation - also the biological limitations are kept in mind. This knowledge sometimes gets lost as the applications diverge from the objective of original data. It was therefore found formative to combine in one volume background information of both the measuring systems and the objects of investigation with the methodology that leads to applications. Newcomers and students in this field may also be interested in how research can be organized to validate and support the inferred information by corroborative measurements made at the surface. Experiences gained during field experiments therefore are described to some detail and useful supplemental information is given in appendices.

Amsterdam Berlin München Firenze Karlsruhe Napoli Oegstgeest Paris Valencia

August 2006

The Editors

Acknowledgements

Most of the results reported here originate from a series of EC projects that started in 1987 with *Remote Sensing of Energy and Mass Exchanges at the Surface of the Earth* (Twinning project no. ST 2 J 0222) and continued with *The ECHIVAL Field Experiment in a Desertification-threatened Area - EFEDA* (EPOC-CT 90-0030), *Remote Sensing and Radiometric Properties of the Surface: Assessment of Desertification from Space - EFEDA Phase II* (EV5V-CT93-0284), *An Integrated Monitoring and Modelling Study of Desertification and Climatic Change Impacts in the Messara Valley of Crete* (EV5V-CT94-0466), *Remote Sensing of Mediterranean Desertification and Environmental Changes - RESMEDES* (ENV4-CT95-0094), and finally *Synthesis of Change Detection Parameters Into A Land-surface Change Indicator for Long Term Desertification Studies in the Mediterranean Area - RESYSMED* (ENV4-CT97-0683). EFEDA was launched by the EC under the Directorate of Scientific Research and Development, Director R.Fantechi, as European contribution to the International Satellite Land-surface Climatology Project (ISLSCP) which was established 1983 and developed its momentum at the International ISLSCP Conference held in Rome, December 1985. The activities were continued under the Director for Research, C. Patermann, and the Head of the Unit for Global Change, DG Research, A. Ghazi, about whose early death in 2005 we deeply mourn for. The projects were supervised by the Officers P. Balabanis and D. Peter

The research community participating in the European activities is deeply indebted to the EC for sponsoring this research into which in addition substantial national funds were invested from the participating countries. More than 35 research groups, including one of the U.S.A., participated in this research of which about one half used satellite data. The book is a recognition of the dedicated work of the many scientists, technicians and administrators that led these EC projects to success. The list of authors includes those scientists, who, in addition to the editors, wrote substantial parts of the book. They were supported as documented in the official project reports by the work of many colleagues to whom editors and authors express their sincere thanks.

These are, in addition to the editors and authors, the initial EFEDA participants: J.-C. André, J. L. Arrué, H. K. Barth, G. Bergkamp, P. Bessemoulin, A. Brasa, J. Bromley, H. A. R. de Bruin, J. Cruces, G. Dugdale, E. T. Engman, D. L. Evans, F. Fiedler, G. Folloni, J.-P. Goutorbe, R. Harding, A. C. Imeson, A.M. Jochum, P. Kabat, T. Kratzsch, J. P. Lagouarde, I. Langer, R. Llamas, L. S. Muniosguren, J. Noilhan, H. R. Oliver, R. Roth, S. S. Saatchi, J. Sanchez Diaz, F. Martin de Santa Olalla, W. J. Shuttleworth, H. Sogaard, H. Stricker, J. Thornes, E. Todini, I.

Vardavas, M. Vauclin, and D. Wickland. Special thanks go to Jutta Wedel for administering the sequence of projects over many years.

In addition we would like to thank the following colleagues who have contributed to reports from which the authors have drawn information, and for assisting editors and authors in many other ways: W. G. M. Bastiaanssen, M. Berger, F. H. Berger, M. Bindi, G. Bitelli, K. Blümel, L. Bottai, J. Cermak, M. Chiesi, R. A. M. De Jeu, J. J. De Vries, P. Dubois, M. Frezzotti, B. T. Gouweleeuw, R. Haverkamp, G. Markl, C. Martellacci, M. Owe, G. Pandiscia, E. Parlow, H. Pelgrum, S. W. M. Peters, D. Praetorius, G. Rana, A. Raschi, F. Rembold, G. Roerink, H. Schmidt, E. Seyhan, B. J. M. Van den Hurk, J. Van Zyl, A. Verhoef and many others who collaborated over the years with editors and authors. We would like to include in our thanks the technical staff and students who build the basis for the extensive field experiments and the data evaluation.

Our gratitude goes to the local administrators who helped to establish the necessary logistic and especially to the land owners who generously allowed their land to be used for the installation the measuring devices and the execution of field measurements.

We acknowledge the support provided by national research establishments and founding organizations which built the basis to receive EC funds and to carry out the large experiment in Castilla-La Mancha and the following evaluationod the data. Spanish researchers are especially thankful to the Regional Ministry for Environment (Directorate General for Environmental Quality) for the maintenance of the Valencia Anchor Station station which is the result of an infrastructure project co-financed by the Regional Government of the Valencia Region and the University of Valencia. The land was indefinitely lent by Bodegas Iranzo and acknowledge also the support provided by the Town Halls of Utiel and of Caudete de las Fuentes. Also thankfully acknowledged is the confidence and scientific support from the GIST (GERB International Science Team) and the SMOS Science Team who count on the Valencia Anchor Station as a reference station for their validation activities, the generous PAPS acquisitions over the validation site by the CERES Science Team and the current collaboration of the Spanish Institute for Meteorology, Institute for Space Studies of Catalonia, Polytechnic University of Catalonia and Field Radiometry Group of the University of Valencia.

Contents

Symbols

Symbol	Definition	Dimension, Value
↓	downwelling (incident) radiation flux	-
↑	upwelling (reflected) radiation flux	-
*	" net" in connection with fluxes	-
α	penetration depth (of heat wave in soils)	m
α	line halfwidth	cm^{-1}
α	absorptance (Φ_a/Φ_0)	-
α	polarizability	A s m^2 V^{-1}
β	Bowen ratio (Φ_{SH}/Φ_{LH})	-
γ	aerosol type factor	-
γ	psychometric constant	0.67 hPa K^{-1} at STP
$\gamma\ (\zeta)$	instrumental response factor for direct solar radiation	-
γ_m	mean atmospheric temperature gradient	K m^{-1}
δ_λ, $\delta(\lambda)$	(vertical)optical depth at wavelength λ of scattering (δ_{scat}) and Rayleigh (δ_R) atmospheres	-
ΔT	temperature amplitude	K
ε	specific kinetic energy dissipation	m^2s^{-3}
ε	permittivity, dielectric constant	A s V^{-1} m^{-1}
ε	emissivity ($M/M_{Black\ Body}$); $\varepsilon_{\mu w}$ microwave emissivity, ε_{IR} thermal infrared emissivity	-
ε_0	permittivity of vacuum	$8.8542 \cdot 10^{-12}$ F m^{-1} = A s V^{-1} m^{-1}
ζ	$\equiv \zeta_{sun}$, solar zenith angle	degree
η	characteristic length of the inner scale (turbulence theory)	mm
ϑ'	zenith angle of the reflected radiation	degree

ϑ	zenith angle of the received radiation	degree
ϑ_{obs}	observation nadir angle	degree
θ	temperature in degree Celsius	°C
θ	specific volumetric soil water content	$m^3\ m^{-3}$
$\varkappa$	instrumental response factor for diffuse radiation	-
$\varkappa$	attenuation index, extinction coefficient	-
λ	wavelength	nm, µm
λ'	local longitude	degree
λ_{ref}	longitude from where the reference time is counted	degree
μ_0, (μ)	cosine of solar(observation) angle	-
μ	magnetic permeability	$V\ A^{-1}\ s\ m^{-1}$
μ_0	permeability of vacuum	$1.25664 \cdot 10^{-6}$ $H\ m^{-1} = V\ s\ A^{-1}\ m^{-1}$
ν	kinematic viscosity	$m^2\ s^{-1}$
$\prod \varepsilon_i^{ai}$	temperature Independent Spectral Index (TISI)	-
ρ $[\rho(\lambda), \rho_\lambda]$	general symbol for reflectance [spectral reflectance] and albedo (Φ_r/Φ_0) [spectral albedo] [1])	-
$\rho(\Omega, \Omega')$	BDRF (Bi-Directional Reflection Factor)	-
$\rho(d\Omega, d\Omega')$	BRDF (Bi-directional Reflectance Distribution Function)	sr^{-1}
$\rho(z)$	air density at height z above mean sea level	$kg\ m^{-3}$
ρ_{air}, ρ	dry air density (0.06% CO_2) $[1.2932/(1+0.00367\ \theta)](p/p_0)$	1226 $kg\ m^{-3}$ at 15°C, 1013 hPa
ρ_p	planetary albedo	-
ρ_{sa}	spherical albedo of the atmosphere	-
σ	specific conductivity	$A\ V^{-1}\ m^{-1}$
$\sigma_R(\vartheta)$	Rayleigh scattering coefficient	$1.06 \cdot 10^{-8}\ \lambda^{-4.09}\ m^{-1}$
τ	transmittance (Φ_t/Φ_0)	-
$\tau_\lambda(m)$	transmittance at wavelength λ and airmass m	-
τ_{atm}	transmittance of the atmosphere	-
φ_{sun}, φ_{obs}	azimuth angle of sun and observation	degree
φ', (φ)	azimuth angle of observed (incident) radiation	degree

Φ	flux	W m^{-2}
Φ_H	buancy flux (flux of turbulent energy)	W m^{-2}
Φ_{LH}, LH	latent heat flux, evaporation	W m^{-2}
Φ_R, R	radiation flux	W m^{-2}
Φ_{SH}, SH	sensible heat flux	W m^{-2}
Φ_{soil}, G	soil (ground) heat flux	W m^{-2}
Ψ	matric potential or suction (soil water pressure/specific weight of water)	Pa kg^{-1} m^2 s^2 = m
ω	$= 15[t_{ref} + (\lambda' - \lambda_{ref})/15 + Z - 12]$, hour angle	hours
ω	circular frequency ($2\pi/N$)	s^{-1}
$\tilde{\omega}$	single scattering albedo	-
Ω	solid angle (into which radiation is reflected)	sr
Ω'	solid angle from which a target receives radiation	sr
a	absolute humidity	kg m^{-3}
a	$= 4\pi\varkappa/\lambda$ absorption coefficient	m^{-1}
A	area (m^{-2})	m^{-2}
A	area	m^2
$A0$	offset coefficient or spectral radiance at QCAL = 0	W m^{-2} sr^{-1}
$A0_\lambda$	post-calibration offset coefficient	mW cm^{-2} sr^{-1} μm^{-1}
$A1$	gain coefficient in units of	W m^{-2} sr^{-1}
$A1_\lambda$	post-calibration gain coefficient	mW cm^{-2} sr^{-1} μm^{-1} DN^{-1}
$\boldsymbol{B}$	magnetic flux density vector	T = kg A^{-1} s^{-2}
$B(T)$	$= L_{BB}(T)$ black body radiance	W m^{-2} sr^{-1}
c	speed of light in vacuum	$2.997925 \cdot 10^8$ ms^{-1}
c	specific heat capacity of soils	J kg^{-1} K^{-1}
c_p	specific heat at constant pressure of air	1005 J kg^{-1} K^{-1}
c_1	$= 2\pi hc^2$, first Planck radiation constant	$3.7418 \cdot 10^{-16}$ Wm^2
c_2	= hc/k, second Planck radiation constant	$1.4388 \cdot 10^{-2}$ mK,
C_n^2	structure parameter (or constant) of the refractive index of air	$m^{-2/3}$
C_u^2	structure parameter for velocity	$(m/s)^2$ $m^{-2/3}$

C_L, C_M, C_H	fractional cloud cover for low, middle and high clouds	-
C_s	volumetric heat capacity	J m^{-3} K^{-1}
d	instantaneous Sun-Earth distance	km
d	path length	m
$\bar{d}$	1 Astronomical Unit (A. U., mean Sun-Earth distance)	$1.496 \cdot 10^8$ km
$d\varepsilon$	vegetation structure parameter	-
D	structural function	m^2 s^{-2}
$\boldsymbol{D}$	displacement vector	C m^{-2} = A s m^{-2}
D	$= \lambda C_s^{-1}$, thermal diffusivity	m^2 s^{-1}
e	water vapour pressure	hPa
e_0	saturation water vapour pressure	hPa
$\boldsymbol{E}$	electric field strength vector	V m^{-1}
E	irradiance (at a target)	Wm^{-2}
f	Cabannes factor	1.054
f	areal fraction covered by vegetation	-
$F_i(\lambda)$	filter function	-
g	acceleration due to gravity	9.8062 m s^{-2} at 45 ° latitude
g_i	weight	-
h	empirical roughness parameter	m
h	height	m
h	Planck constant	$6.6262 \cdot 10^{-34}$ J s,
H	index, horizontal polarization	-
$\boldsymbol{H}$	magnetic field strength vector	A m^{-1}
H	$= RT_0/Mg$, scale height	8435 m
H_d	extraterrestrial solar radiant exposure (irradiance at a horizontal plane integrated over specified exposure time)	J m^{-2} day^{-1}
i	(index) isotropically reflecting (Lambertian) surface	-
i	index denotes spectral channel	-
I	$= (\rho c \lambda \omega)^{1/2}$, thermal inertia	W m^{-2} K^{-1}

k	time constant of clear sky surface temperature post maximum exponential decay	hours
k	$= 2\pi/\lambda$ wavenumber	m^{-1}, nm^{-1}, μm^{-1}
k	von Kármán constant	0.4
k	Boltzmann constant	$1.3807 \cdot 10^{-23}$ JK^{-1}
K	force constant	N m^{-1}
$K(\theta)$	hydraulic (or capillary) conductivity	m s^{-1}
L	latent heat of water vaporization (A.5)	≈2.465 MJ kg^{-1} at 15°C
L	radiance	$Wm^{-2}sr^{-1}$
L_λ	spectral radiance	mW cm^{-2} sr^{-1} μm^{-1}
$LMAX_\lambda$	maximum spectral radiance	mW cm^{-2} $ster^{-1}$ μ at QCAL = 255 DN
$LMIN_\lambda$	minimum spectral radiance	mW cm^{-2} $ster^{-1}$ μm at QCAL= 0 DN
L_{MO}	$= - c_p\, T_v\, \rho\, u_*^3 / g\, k\, \Phi_H$, Monin-Obukhov length	m
m	mass	kg
m	relative airmass	-
M	radiation flux density across a unit area	Wm^{-2}
M_a	molar mass of air up to about 90 km	0.028964 kg $mole^{-1}$
n	refractive index	-
n	index “natural” reflector	-
N	molecules per unit volume	m^{-3}
N	number of molecules per unit volume (Loschmidt number)	$2.6867 \cdot 10^{25}$ m^{-3}
n_0	refractive index of air at 700 nm and sea level	$2.76 \cdot 10^{-4}$
p	pressure of air	hPa
$\boldsymbol{p}$, $\boldsymbol{P}$	electric dipole momentum	A s m
P_v	fractional vegetation cover	-
p_0	standard air pressure	1013.25 hPa
Ph	energy consumed for photosynthesis	W m^{-2}
$p_R(\vartheta)$	Rayleigh scattering phase function	-
q	specific humidity	g kg^{-1}

$QCAL$	quantised and calibrated scaled radiance	DN
$q_l^*(T)$	the temperature dependent value of the specific humidity at saturation that is assumed to be reached within the leaves	g kg^{-1}
q_s	the specific humidity at the bare soil surface or if this is dry	g kg^{-1}
$q_s\,(SST)$	specific humidity at saturation defined by the sea surface temperatur	g kg^{-1}
$\mathbf{r}$	position vector	m
r	resistance to energy transfer r_a aerodynamic resistance, r_s resistance of unsaturated soil, r_{st} stomatal resistance	s m^{-1}
R	gas constant	8.314 J mole^{-1} K^{-1}
R	mean earth radius	6356766 m
R_0	range (ΔR_0 pixel size)	m
$S\,(T)$	line strength (integrated absorption)	cm^{-1} sec^{-1}
S_0	exo-atmospheric solar flux density ("solar constant")	1368±1 W m^{-2}
$S_\lambda\,(\varphi,\delta,t)$	solar spectral flux density at the top of the atmosphere at latitude φ, declination δ and time t through a horizontal surface	W m^{-2} µm
T	temperature	K
T	$= \delta_{scat}/\delta_R$, turbidity factor (Linke)	-
t_{ref}	reference time, time in hours measured in zonal mean time	hours
$t(T_m)$	time of clear sky surface temperature maximum	hours
T_0	reference temperature, e.g. 288.15 K (15 °C)	K
T_{BB}	black body emission temperature	K
T_{eff}	effective radiative surface temperature	K
T_v	$= T(1+0.61q)$, virtual temperature	K
u_{10}	wind speed at 10m height	m s^{-1}
u_*	friction velocity	m s^{-1}
V	index, vertical polarization	-
w	precipitable amount of water vapour	cm
W	band-width	µm

W	equivalent width	cm^{-1}
z_0	roughness length	cm
z_{ref}	reference height	m
Z	equation of time	hours

[1]) Use of the reflectance symbol ρ:

Symbol	Definition	Dim.
ρ (dΩ, dΩ')	bi-directional [spectral] reflectance distribution function (BRDF), ratio of the directional radiance (W m^{-2} sr^{-1}) reflected from a target within an infinitesimally narrow solid angle to the incident flux density (irradiance, W m^{-1}) generated by a point source	sr^{-1}
ρ (Ω, Ω') [ρ_λ (Ω, Ω')]	bi-directional [spectral] reflectance factor (BDRF) defined as ratio of the radiance reflected from a target to that one reflected from a white Lambertian reference panel under identical illumination and observation conditions. The directional radiance originating from a white Lambertian surface equals 1/π of its irradiance. The BRDF therefore can be expressed as (radiance target)/(π·radiance reference) or π·BRDF = BDRF	-
ρ (dΩ, 2π)	ratio of directional radiance reflected from a target to the irradiance from a hemispherical source(directional-hemispherical reflectance)	sr^{-1}
ρ (2π, 2π)	albedo (= bi-hemispherical reflectance factor): ratio of hemispherically reflected to incident radiation flux (sometimes the overbar $\bar{\rho}$ is used to indicate broad band albedo)	-

Chapter 1 Introduction

1.1 Space View and Ground Observations

The approach followed in this publication is based upon available long term data series of NOAA-AVHRR and Nimbus-SMMR and occasional Landsat-TM, SPOT, Meteosat, and ERS1/2 scenes. The spectrum ranges from the visible to microwaves. This broad approach was found to be advantageous for the following reasons: (i) information inferred from medium resolution satellite data can be validated by stepwise scaling up from point measurements made at the ground first to high resolution satellite data and then, by aggregation of pixels, to measurements made by NOAA-AVHRR and Meteosat, (ii) the different observation times and different spatial resolutions of satellite systems supplement each other, and (iii) information gained from sensors with different spectral characteristic mutually support each other. For the entire lifetime of the new European Envisat mission, for example, measurements from a variety of instruments are simultaneously available for the first time. This, nowadays greatly enhances the synergy effect of the measurements.

Most of the presented data result from research projects of the European Commission, DG Research, starting 1991 with the ECHIVAL[1] Field Experiment in Desertification-threatened Areas (EFEDA)[2]. These projects were initiated to study the causes of land degradation and desertification, their relationship to climate change and man's activities, and to develop indices to quantify these changes. One aim was to explore the role which observations from space can play to analyse the processes that occur at the land surfaces and to overview the whole Mediterranean basin. Because of the complex topographical structure of the Mediterranean landscape it seems impossible to obtain such an overview for a longer time period exclusively by measurements at the surface. Long term observations are necessary to assess trends superimposed by large annual fluctuations as is the case in the Mediterranean area. Some climate state variables indicate a quasi-periodicity of about 23 years. Consequently the aim must be to extend the use of measurements from space to such time scales. Because different satellites with varying instruments must be used to cover such a long period, great care has to be taken to construct homogeneous data series. Only then the analysis of remote sensing data gains weight

---

[1]European International Project on Climatic and Hydrological Interactions between Vegetation, Atmosphere, and Land-surfaces

[2]A short description of these activities can be found in Appendix 1.

in this research. The outcome for the Mediterranean area may also be useful for investigations and applications in other parts of the world.

The remote sensing component of the above mentioned EC research projects did not aim at an assessment of land-surface changes by means of repetitive classification of land-use units. They were rather meant to relate measurements from satellites to physical and biological quantities that drive land surface - atmosphere interactions and change due to man's activities and climate variability. One important question is whether these processes may be subject to irreversible trends due to global change.

Changes at the land surfaces are driven by the annual sequence of weather situations, extreme weather events, long term global climate change, and the activities of man in response to ecological and economical forcing. The various processes involved are briefly reviewed in the following sections of this introduction.

1.2 Mediterranean Climatic Environment

Mediterranean climate occurs in a number of western continental coasts between 30° and 45° north and south (Strahler 1975). Research in the about 4 Mkm^2 large European, African and Levantine land masses around the Mediterranean Sea therefore finds its congruity in other regions of the world, such as at the fringe of the subtropics in the south-west of the United States, Mexico, Chile, Australia, and South Africa. Notwithstanding this climatic correspondence, the situation of the European-African-Levantine Mediterranean Basin differs in some respect from that of the other Mediterranean regions. Its highly structured landmasses border a nearly closed large inland sea of about 2.5 Mkm^2 stretching over 42° longitude or as much as 3.02 Mkm^2 if, in addition, one counts the Marmora and the Black Seas as part of the Mediterranean area. Because of this longitudinally elongated water mass enclosed by land, the Mediterranean climate stretches further eastward to south of the Caspian Sea. This would enlarge the extend of the Mediterranean area to about 10 Mkm^2, which is unique in the world.

The Mediterranean climate and its variability was recently described by Lionello et al. (eds.) (2005). Here only a few processes are recalled in connection to remote sensing opportunities. The topographically complex Mediterranean Basin, positioned between the subtropical Hadley circulation system[3] and the westerlies, is characterized by strong climatic gradients and several specific phenomena (see Fig A.2.1 in Appendix 2). The latter are caused by the seasonal variability of the latitudinal position of the "polar front", land-sea circulation systems, travelling cyclones, low pressure systems caused by convection from hot surfaces, and across and around mountain air-flows. Mineral dust from the neighboured Saharan desert as well as from Mediterranean areas with bare soils and air pollution generated locally or imported from central Europe are blown over the area. The Mediterranean basin therefore is ideal for research into the interaction of processes between land,

[3]Meteorological terms used in this book are explained in Appendix 2

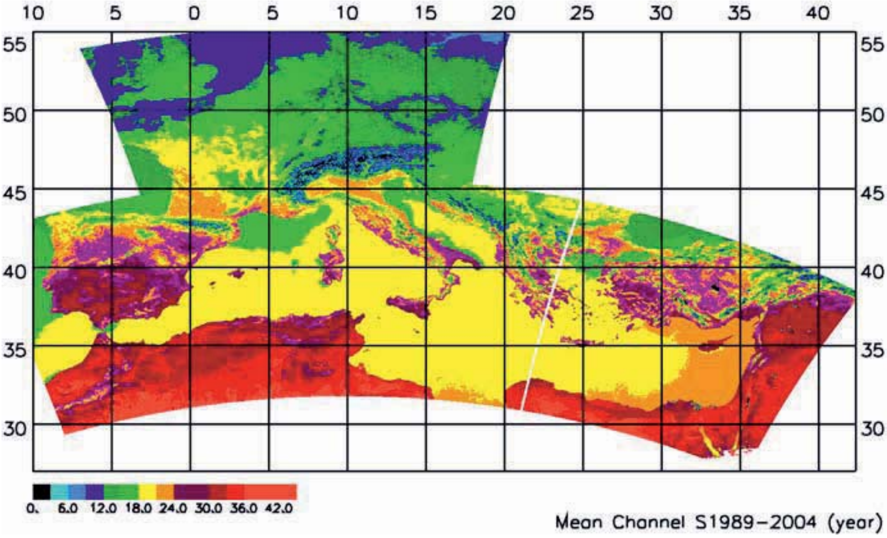

Fig. 1.1. Long term 1989 - 2004 annual mean of the radiative surface temperature for cloudless days and at the time of the NOAA satellites overpasses (the scale is in °C)

atmosphere and sea under variable climatic conditions and at different scales.

The south - north climate gradient shows up in measurements of the radiance in the thermal infrared spectral bands converted to equivalent temperatures at the top of the atmosphere (TOA) and then corrected with the split-window technique for atmospheric effects. The annual mean temperature averaged over the years 1989 to 2004 as obtained by the AVHRR instrument for cloudless days at the time of the NOAA satellite overpass (e. g. nominal 15:50 UT for NOAA-14 which was the same for NOAA-11 at launch but by March 1995 NOAA-11 had drifted to 17:33 UT) is shown in Fig. 1.1. Seasonally averaged TOA temperatures for cloudless conditions during the years 1989 - 1998 are presented in section 6.9. The colours indicate temperatures in steps of five degrees ranging from black (0 °C) to red (≥ 42 °C).

Higher spatial resolution is obtained with Landsat-TM images as shown for south-western Tuscany in Fig. 1.2. Here, the relationship between surface temperature and land cover (but also altitude) becomes evident. Areas with a high vegetation index are cooler than harvested fields or quarries with normalized difference vegetation indices (section 4.6) of typically < 0.2 that indicate bare soils. Most of the high vegetation index sites are at hills which in addition are affected at their windward side by the sea breeze. Solar radiation at inclined hilly terrain, various types of land-use, and the sea breeze cause a diversity of microclimates.

The average land-surface maximum temperature gradient across the basin is of the order of 20 K. As Fig. 1.2 shows, temperature differences of this magnitude also occur at single days in heterogeneous terrain. During winter, the southern European countries are close to sea surface temperature near noon and, therefore, one can hardly detect the coastlines in thermal infrared satellite images (see Fig. 6.9.1). In spring, lowlands and bare to sparsely vegetated plateaux heat up first. During summer, the heat is nearly equally distributed across the basin though the North African and Levantine areas are on average about 15 K warmer than the most southern European countries. In autumn, the south of Spain, the Anatolian highlands, the east of Greece, the chain of central Mediterranean Islands and Puglia remain warm longer than the rest of southern Europe which tends towards the SST. The contrast between mountainous areas and plains is considerable. This leads to locally complex valley-mountain circulation systems or katabatic winds as known for the north-eastern Adriatic coast, where cold air descends from the mountains to sea level ("Bora"). Though regional contrasts show up in these pictures nearly the same way every year, the average temperature level may change from year to year. As an example, in autumn 1998 Anatolian highlands were remarkably warmer than in 1997 and 1999 (see section 6.9.1).

The sea surface temperatures (SST) of the Mediterranean Sea show spatial differences up to 15 K as can be seen in a more distinctive manner for a summer month taken by ATSR (for satellite and instruments specifications see Chapter 2 and Appendix 4) on ERS-2 (Fig. 1.3). There are different reasons that lead to a patchy distribution of the SST: Differential solar heating, upwelling of cooler deep water due to internal circulations, water exchange with the Atlantic Ocean, run-off of cooler river water into the sea, and the intrusion of water from the Black Sea through the Sea of Marmara. A cold water surge into the Aegean in some years occurs in the early spring when the Black Sea has the lowest temperatures in the region due to the inflow of water from northern rivers. On an annual basis, the general features of the SST reappear year by year. During summer, the central and eastern parts of the sea are warmer than the western part and the Aegean.

During winter, vigorous synoptic scale weather systems imbedded in the westerlies are the overriding weather phenomena. High mountain barriers such as the Atlas, the Pyrenees, the Alps, and the Balkan mountains modify or even generate these weather systems which develop in the middle troposphere and gain their momentum by internal energy transfer processes. Well known is the Genova cyclone generated by the interaction of the westerly airstream with the bow of the Alps. Behind higher mountains often chinook-like pattern ("Föhn") develop. Smaller topographic obstacles are less important for these synoptic scale processes.

The picture changes completely during summer when the westerlies pass further north and only seldom, in "blocking" situations, affect the Mediterranean area. At this time of the year, mesoscale and regional topographic effects gain in importance and interact with the now much smoother large scale pressure distribution in the Mediterranean area. It is mainly the land-sea circulation that becomes responsible for the exchange of dry and humid air between land and sea. Already during spring, large thermal contrasts build up during daytime between sea and land causing warm air to rise in coastal zones. This generates low surface pressure entraining cooler, wetter, and heavier air from the sea which warms up rapidly when arriving over land.

Uprising may develop into vigorous thunderstorms if the moisture is available to generate deep convective systems that are fed by the latent heat. The air over the sea which in summer has surface temperatures of 22 - 27°C, locally even higher, can take up large amounts of water vapour but it often needs additional lifts by near

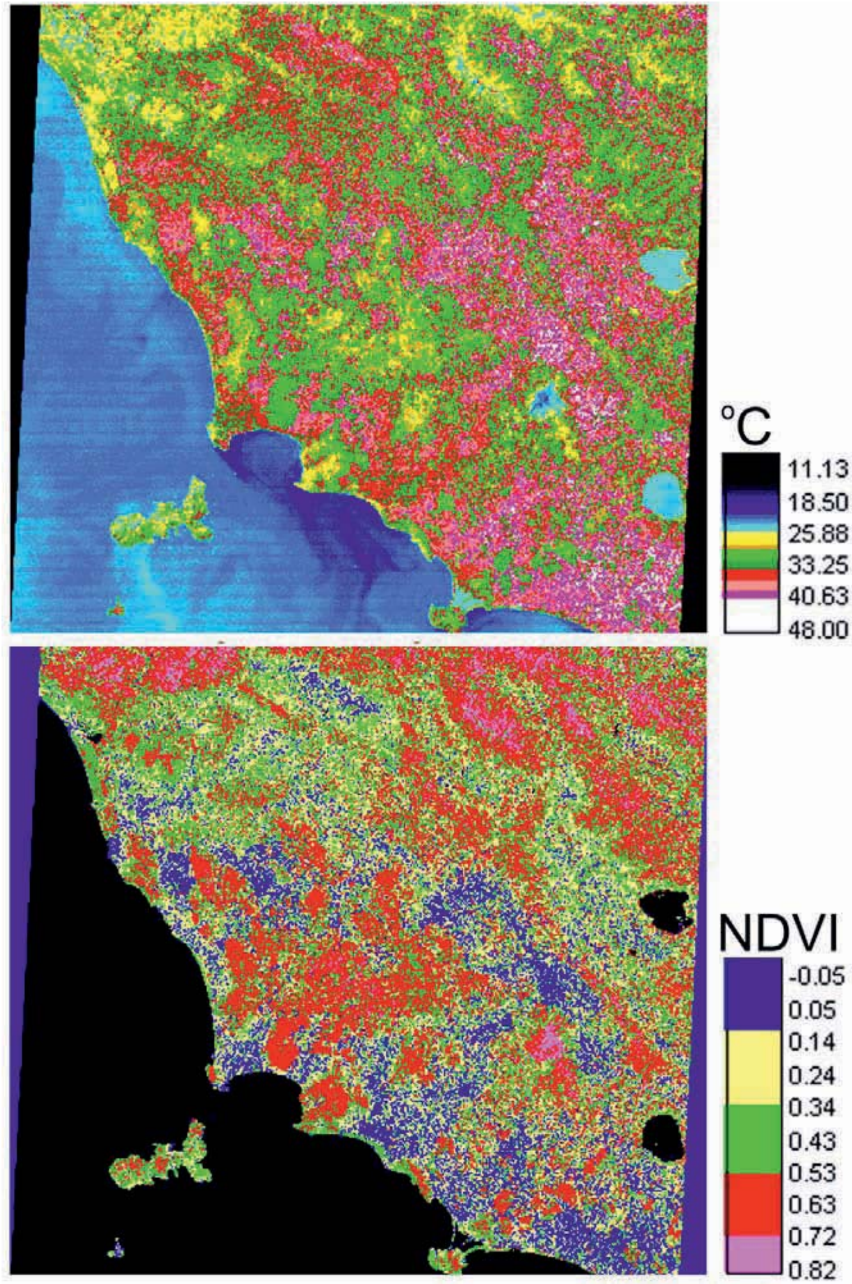

Fig. 1.2. Top: Landsat-TM channel 6 thermal image of south-western Tuscany, 10 August 1998. Colour code on the right in degree Celsius. Bottom: Normalized Difference Vegetation Index (NDVI - normalized near infrared to red signal difference) of the same scene with scale on the right

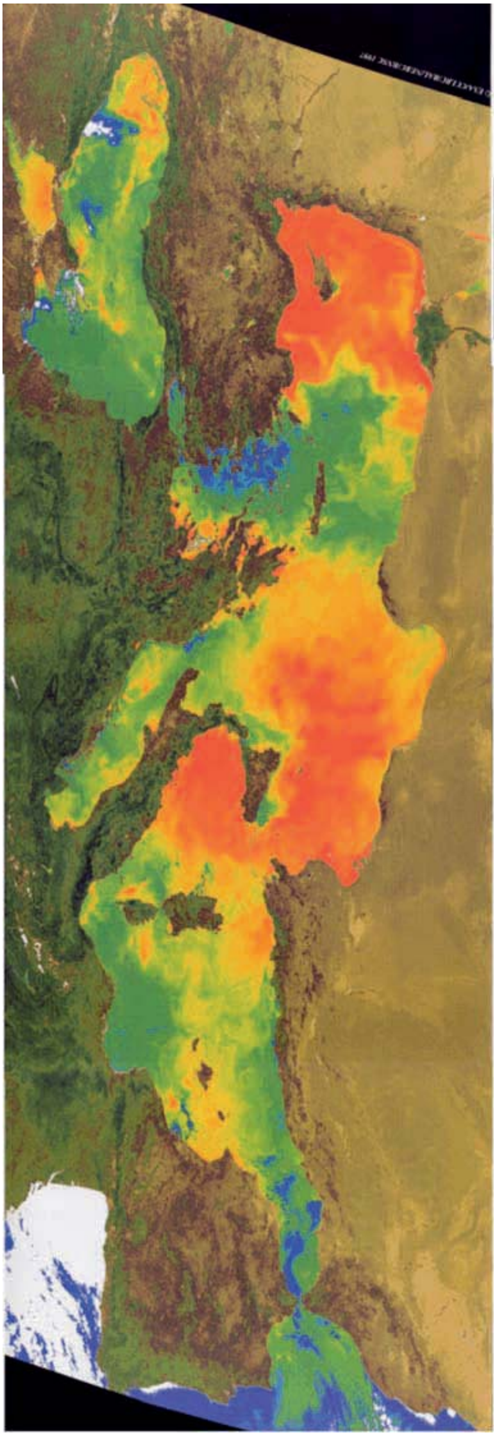

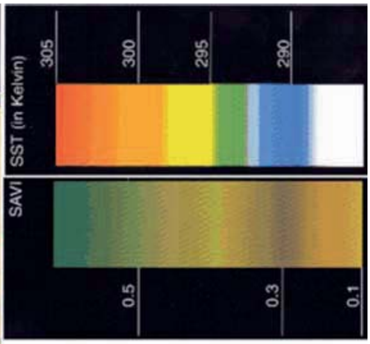

Fig. 1.3. Mediterranean sea surface temperature and vegetation cover over land. The image was derived from 400 scenes of the Along Track Scanning Radiometer (ATSR) on board of the ERS-2 satellite recorded between 17 July and 8 August 1996. The vegetation index used over land is the Soil Adjusted Vegetation Index (SAVI). Courtesy ESA

coastal mountains to move this air up to the condensation level. Pfister (1999) therefore made such local effects responsible for severe floods in the Mediterranean area. These occur often in autumn when the air is cooling more rapidly than the ocean. Millán et al. (1995) and Millán (2000) reported cases of torrential rainfall near Valencia that occurred in autumn when a high pressure cell was over France and a low pressure cell over north-western Africa. The air took up its moisture from very warm water near Tunisia. This was led quickly towards the Spanish coast and released its water when it was lifted upward by the mountains near the coast.

Buzzi et al. (1994, 1998) and Pfister (1999) could attribute such flood events *inter alia* to processes which occurred several days earlier over the North Atlantic Ocean. They found that the atmospheric flow over the North Atlantic and Mediterranean area intensifies as the south to north temperature gradient increases in autumn which would transport considerable additional amounts of moisture into these regions. Pinto et al. (2001) investigated 30 cases of intense rainfall and showed that tropical systems and tropical-extratropical interactions indeed can play an important role in these processes. They detected three mechanisms that may influence the development of extreme Mediterranean precipitation events:

A. Tropical systems over the eastern-central North Atlantic curve directly towards the Mediterranean, undergo a transition into an extra-tropical cyclone and unload their moisture in the western Mediterranean area.

B. Tropical systems over the western and central North Atlantic become extra-tropical cyclones and advect moisture from the subtropics to the extra-tropics. Part of this moisture is then transported by the converted former tropical or other systems along the southern rim of the upper tropospheric main flow towards southern Europe.

C. The tropical system over the western North Atlantic curves east and connects with an approaching upper-tropospheric mid-latitude trough system. The eastern trough of this Rossby wave over the Iberian peninsula induces a south-westerly flow of this moist air over the western Mediterranean area and directs this flow against the south side of the Alps.

The authors investigated in detail the heavy precipitation event of 13-16 October 2000 when the Po level reached record heights. A tropical storm ("Leslie") became an extra-tropical cyclone near Newfoundland. It followed and joined the westerlies and, positioned in a strong baroclinic zone, it crossed the North Atlantic towards the British Isles. Over Spain the general air flow formed a trough which directed a secondary system that inherited part of Leslie's moisture towards the Strait of Gibraltar and from there to the Alps. The updraft due to the mountain barrier then caused the heavy rainfall.

In summer, the westerlies are positioned more northward. Then the these processes do not play a role. Fig. 1.4 gives an impression of phenomena that can be observed in early summer. Over the north-eastern Iberian Peninsula and southern France the development of a large cloud field can be observed that is related to a low pressure system embedded in the north-easterly flow of the westerlies. This is a situation similar to what has been described for the autumn rainfall period but the north-eastward flow occurs more westerly towards France. Over Italy and further east the land-sea circulation leads to cumulus convection over mountain chains such